

Significant improvements of structure and magnetic properties of $\text{Pr}_2\text{Fe}_{14}\text{B}/\alpha\text{-Fe}$ nanocomposite magnets due to Cu and Mn substitution

Bai Yang*, Bao Gen Shen, Tong Yun Zhao, Ji Rong Sun

State Key Laboratory of Magnetism, Institute of Physics and Beijing National Laboratory for Condensed Matter Physics, Institute of Physics, Chinese Academy of Sciences, Beijing 100080, People's Republic of China

Received 15 June 2007; received in revised form 20 August 2007; accepted 8 September 2007

Abstract

The influence of Cu and Mn substitution on the structure and magnetic properties of melt-spun $\text{Pr}_8\text{Fe}_{87-x}\text{B}_5\text{M}_x$ ribbons with $0 \leq x \leq 1.2$ was studied. The experimental results show that the Cu substitution of appropriate quantity leads to the *c*-axis alignment of $\text{Pr}_2\text{Fe}_{14}\text{B}$ phase in melt-spun ribbons. The substitution of Mn improves magnetic properties of melt-spun $\text{Pr}_8\text{Fe}_{87-x}\text{B}_5\text{Mn}_x$ ribbons, but does not show the same influences on the alignment of $\text{Pr}_2\text{Fe}_{14}\text{B}$ phase as Cu substitution does. A remanence of 1.33 T, a coercive field of 462 kA/m and a maximum energy product of 185 kJ/m^3 in $\text{Pr}_8\text{Fe}_{86.4}\text{B}_5\text{Mn}_{0.6}$ ribbons are obtained at room temperature.

© 2007 Elsevier B.V. All rights reserved.

Keywords: Cu and Mn substitution; Melt-spun ribbons; Structure; Magnetic properties

1. Introduction

As predicted by theoretical calculation [1], nanocomposite magnets consisting of hard and soft magnetic phases of nanometric sizes may have potential maximum energy products up to 1 MJ/m^3 . The relatively lower rare earth contents make the nanocomposite magnets higher corrosion resistance and lower in cost. So nanocomposite magnets are considered as another kind of new magnet that may take the place of the traditional rare earth magnets, and attract more research interest of them. But so far the results of experimental research are far from those of calculation, and the actual maximum energy products are about $80\text{--}160 \text{ kJ/m}^3$ for samples prepared through mechanical alloying [2,3] and melt spinning [4,5], which are main preparing methods of nanocomposite magnets. The reasons of large difference between the results of experiment and calculation may lie in three aspects: (1) grain sizes of crystallites of hard and soft phases in nanocomposite magnets prepared in the experiment do not accord with those of calculation, which are about $10\text{--}20 \text{ nm}$; (2) crystallites are distributed not uniformly and their

shapes are not regular; (3) the *c*-axis texture of hard phases such as $\text{Pr}_2\text{Fe}_{14}\text{B}$, is not easily realized. For isotropic nanocomposite magnets, refinement and uniform distribution of the grains in magnets are the important factors that influence the actual magnetic properties [6,7]. Many efforts were made to optimize the microstructure and improve magnetic properties by adding some transition metal or heavy rare earth elements to nanocomposite alloys [8–12], but in all case, H_c of the composites was improved but with a decrease in B_r . It has been reported that crystallographic texture of nanocomposite $\text{Nd}_2\text{Fe}_{14}\text{B}/\alpha\text{-Fe}$ ribbons can be prepared by controlled melt spinning [13]. However, it is difficult to realize ideal anisotropic microstructure for nanocomposite magnets in experiments. Therefore, more attempts should be made to investigate the crystallization process, microstructure and magnetic properties of nanocomposite magnets prepared by melt spinning.

It is reported that the addition of Cu [14] or the combined addition of Cu and Nb [15,16] can lead to the improvement of the magnetic properties of nanocomposite $\text{Nd}_2\text{Fe}_{14}\text{B}/\alpha\text{-Fe}$ melt-spun ribbons after optimal annealing due to the refinement of the microstructure. Additionally, studies have shown that Cu addition can decrease the optimal cooling rate for achieving high coercivity in $\text{Fe}_3\text{B}/\text{Nd}_2\text{Fe}_{14}\text{B}$ -type nanocomposite magnets [17]. But the effect of Cu addition on microstructure and

* Corresponding author. Tel.: +86 10 82648085; fax: +86 10 82649485.
E-mail address: yangbai@g203.iphy.ac.cn (B. Yang).

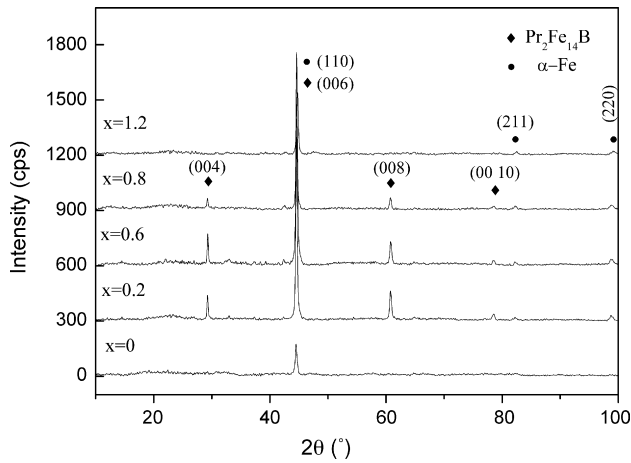


Fig. 1. X-ray diffraction patterns of the free surfaces of $\text{Pr}_8\text{Fe}_{87-x}\text{B}_5\text{Cu}_x$ ($x=0, 0.2, 0.6, 0.8$ and 1.2) ribbons prepared at the optimum wheel speed of 20 m/s.

magnetic properties of melt-spun nanocomposite magnets is still unclear.

In this article, the structure and magnetic properties of melt-spun $\text{Pr}_8\text{Fe}_{87-x}\text{B}_5\text{M}_x$ ($M = \text{Cu}, \text{Mn}$) ribbons are studied. The different effects of the Cu and Mn substitution on structure and magnetic properties of the alloys are analyzed. It is found that an appropriate amount of Cu substitution leads to the c -axis alignment of $\text{Pr}_2\text{Fe}_{14}\text{B}$ phase in melt-spun ribbons, and the substitution of Mn makes the grain sizes of $\text{Pr}_2\text{Fe}_{14}\text{B}$ phase finer and improves magnetic properties of melt-spun $\text{Pr}_8\text{Fe}_{87-x}\text{B}_5\text{Mn}_x$ ribbons.

2. Experimental procedure

The alloy ingots with nominal compositions of $\text{Pr}_8\text{Fe}_{87-x}\text{B}_5\text{M}_x$ ($M = \text{Cu}, \text{Mn}; x = 0, 0.2, 0.4, 0.6, 0.8$ and 1.2) were prepared by electric arc melting in argon atmosphere of high purity. Five weight percent of Pr, more than that of the stoichiometric value, was added to the alloys to compensate for the loss of Pr. Ribbons of these alloys were obtained by melt spinning in argon atmosphere. The substrate velocity of Cu wheel varied from 16 to 25 m/s. The phase composition and structures of melt-spun ribbons were examined by X-ray diffraction (XRD) using $\text{Cu K}\alpha$ radiation. The microstructure of the ribbons was observed by an H-800 transmission electron microscope (TEM). Thermo-magnetic analysis was performed by using a vibrating sample magnetometer (VSM) at a furnace temperature of 900 °C under an applied field of 80 kA/m. The magnetic properties of the samples were measured by a VSM with maximum applied field of 2 T.

3. Results and discussion

Fig. 1 shows the X-ray diffraction patterns of the free surfaces of melt-spun $\text{Pr}_8\text{Fe}_{87-x}\text{B}_5\text{Cu}_x$ ($x = 0-1.2$) ribbons prepared at the optimum wheel speed of 20 m/s. It is found that $\text{Pr}_2\text{Fe}_{14}\text{B}/\alpha\text{-Fe}$ type nanocomposite microstructure was formed directly during melt spinning. Strong alignment of $\text{Pr}_2\text{Fe}_{14}\text{B}$ phase with reflections of indices of (004), (008) and (0010)

is observed with $x = 0.2-0.8$, and the (110) reflection of $\alpha\text{-Fe}$ is much stronger, which overlaps the (006) reflection of $\text{Pr}_2\text{Fe}_{14}\text{B}$. The pure c -axis texture of $\text{Pr}_2\text{Fe}_{14}\text{B}$ is evidently normal to the free surface of the ribbons with $x = 0.2-0.8$. With $x > 0.8$, the c -axis alignment of $\text{Pr}_2\text{Fe}_{14}\text{B}$ phase with the (00 l) reflections disappears in the ribbon plane. It can be seen that the Cu substitution of appropriate quantity promotes crystallization and c -axis alignment of $\text{Pr}_2\text{Fe}_{14}\text{B}$ phase during melt spinning.

From the XRD patterns of the melt-spun ribbons of $\text{Pr}_8\text{Fe}_{87-x}\text{B}_5\text{Cu}_x$ with $x > 0$, the value of lattice parameter a of $\alpha\text{-Fe}$ in the ribbons is about 0.2886–0.2889 nm, a little larger than that of pure $\alpha\text{-Fe}$ (0.2866 nm). For the characteristic peaks for $\alpha\text{-Fe}$ in $\text{Pr}_8\text{Fe}_{87}\text{B}_5$ ribbons is undistinguishable in the patterns, the lattice parameters of pure $\alpha\text{-Fe}$ phase is not determined by the XRD patterns but referred to a standard PDF card for pure $\alpha\text{-Fe}$ (PDF number: 06-0696) published by JCPDS-International Center for Diffraction Data in 1999. This implies that in the process of melt spinning, a little amount of Cu probably dissolves in $\alpha\text{-Fe}$. The possible reasons of c -axis alignment of $\text{Pr}_2\text{Fe}_{14}\text{B}$ phase in the $\text{Pr}_8\text{Fe}_{87-x}\text{B}_5\text{Cu}_x$ ribbons may base on the location of Cu in $\alpha\text{-Fe}$. Since the nucleation and growth of both $\text{Pr}_2\text{Fe}_{14}\text{B}$ phase and $\alpha\text{-Fe}$ phase are determined by the atomic diffusion, the existence of Fe in two phases would make them crystallize and grow up competitively during solidification. The retarded growth of $\alpha\text{-Fe}$ would trigger the nucleation and texture growth of $\text{Pr}_2\text{Fe}_{14}\text{B}$ phase. Our experimental results have shown that the pure c -axis texture of $\text{Pr}_2\text{Fe}_{14}\text{B}$ is observed in Cu-doped ribbons spun at high speed of 20 m/s. We believe that this may be ascribed to the influences of Cu substitution on the process of rapid solidification of $\text{Pr}_8\text{Fe}_{87-x}\text{B}_5\text{Cu}_x$ alloys. As is known, melt spinning is a nonequilibrium solidification process, in which the supercooling of melt alloys has a strong impact on crystallization process of the alloys. From the above, we deduce that a little amount of Cu in the Fe phase possibly increase the supercooling of $\alpha\text{-Fe}$ during rapid solidification, and restrain the crystallization and growth of $\alpha\text{-Fe}$. The postponed growth of $\alpha\text{-Fe}$ make $\text{Pr}_2\text{Fe}_{14}\text{B}$ phase competitively crystallize and grow up in solidification. In the phase diagram of Fe–Cu, the solubility of Cu in $\alpha\text{-Fe}$ is about 0.6 at.% at room temperature. In the alloys of $\text{Pr}_8\text{Fe}_{87-x}\text{B}_5\text{Cu}_x$ with $x > 0.6$, besides the solubility of Cu in $\alpha\text{-Fe}$, the redundant amount of Cu possibly crystallizes before $\alpha\text{-Fe}$ and $\text{Pr}_2\text{Fe}_{14}\text{B}$ phase, and exists surrounding such phases to prohibit the growth of them. So with more additions of Cu, there is no c -axis alignment of $\text{Pr}_2\text{Fe}_{14}\text{B}$ phase in the $\text{Pr}_8\text{Fe}_{87-x}\text{B}_5\text{Cu}_x$ ribbons. From grain sizes estimated by X-ray reflection broadening by the Scherrer formula, it also can be seen that the average grain size of $\text{Pr}_2\text{Fe}_{14}\text{B}$ in $\text{Pr}_8\text{Fe}_{85.8}\text{B}_5\text{Cu}_{1.2}$ ribbons at speed of 20 m/s is about 20 nm, while those of $\text{Pr}_2\text{Fe}_{14}\text{B}$ with the c -axis alignment is about 30–40 nm.

Our further experiments show that there is no c -axis alignment in the roller surface of ribbons so that texture of $\text{Pr}_2\text{Fe}_{14}\text{B}$ phase in the free surface does not penetrate through the thickness of melt-spun ribbons because of high cooling rate in the roller surface. From the above results, it can be concluded that during melt spinning the formation of c -axis texture of $\text{Pr}_2\text{Fe}_{14}\text{B}$ begins in the free surface.

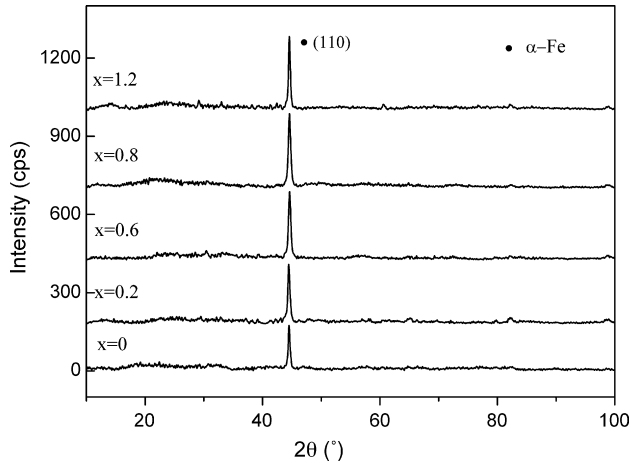


Fig. 2. X-ray diffraction patterns of the free surfaces of $\text{Pr}_8\text{Fe}_{87-x}\text{B}_5\text{Mn}_x$ ($x=0, 0.2, 0.6, 0.8$ and 1.2) ribbons prepared at the optimum wheel speed of 20 m/s.

Fig. 2 shows the X-ray diffraction patterns of the free surface of melt-spun $\text{Pr}_8\text{Fe}_{87-x}\text{B}_5\text{Mn}_x$ ($x=0-1.2$) ribbons prepared at the optimum wheel speed of 20 m/s, which show nanocomposite microstructures different from those of the melt-spun ribbons of $\text{Pr}_8\text{Fe}_{87-x}\text{B}_5\text{Cu}_x$. In Fig. 2, no c -axis orientation of $\text{Pr}_2\text{Fe}_{14}\text{B}$ phase but the (1 1 0) reflection of α -Fe is observed.

The representative dark-field TEM micrographs of grain morphology of the $\text{Pr}_8\text{Fe}_{86.4}\text{B}_5\text{Cu}_{0.6}$ and $\text{Pr}_8\text{Fe}_{86.4}\text{B}_5\text{Mn}_{0.6}$ ribbons prepared at the optimum wheel speed of 20 m/s are presented in Fig. 3. It indicates that the Cu-doped ribbons have a coarse microstructure consisting of large $\text{Pr}_2\text{Fe}_{14}\text{B}$ and α -Fe grains

with an average size of 30–40 nm. Some oriented $\text{Pr}_2\text{Fe}_{14}\text{B}$ crystals having a columnar characteristic with a grain size of about 60 nm can be observed. A homogeneous microstructure with ultrafine grains is observed in $\text{Pr}_8\text{Fe}_{86.4}\text{B}_5\text{Mn}_{0.6}$ ribbons in Fig. 3(b). The substitution of Mn does not have the same effect on microstructure of melt-spun ribbons as Cu substitution does, the cause of which likely lies in different influences of Cu and Mn substitution on the process of rapid solidification of $\text{Pr}_8\text{Fe}_{87}\text{B}_5$ alloys.

One may notice that the diffraction peaks of the 2:14:1 phase in melt-spun $\text{Pr}_8\text{Fe}_{87-x}\text{B}_5\text{Mn}_x$ ribbons are not obviously detected in comparison with those of Cu-doped ribbons. For further investigation of the existence of 2:14:1 phase, we have measured the temperature dependence of magnetization of melt-spun $\text{Pr}_8\text{Fe}_{87-x}\text{B}_5\text{Mn}_x$ ribbons with $x=0$ and 0.6 under an applied field of 80 kA/m, as shown in Fig. 4. It can be found that there are two onsets in the $M-T$ curves, and besides one set at about 780 °C corresponding to α -Fe phase, a set at about 330 °C are observed, indicative of the existence of the $\text{Pr}_2\text{Fe}_{14}\text{B}$ phase in melt-spun $\text{Pr}_8\text{Fe}_{87-x}\text{B}_5\text{Mn}_x$ alloys. The HRTEM image or select-area electron diffraction (SAED) may present the existence and morphology of 2:14:1 phase better, but the H-800 transmission electron microscope (TEM) used in our experiment cannot perform these items. A high-level TEM will be used in our future work.

Fig. 5 shows the room-temperature coercive field iH_c , remanence B_r and maximum energy product $(BH)_{\max}$ of melt-spun $\text{Pr}_8\text{Fe}_{87-x}\text{B}_5\text{M}_x$ ($M=\text{Cu}, \text{Mn}$) ribbons prepared at the optimum wheel speed of 20 m/s as a function of M concentration

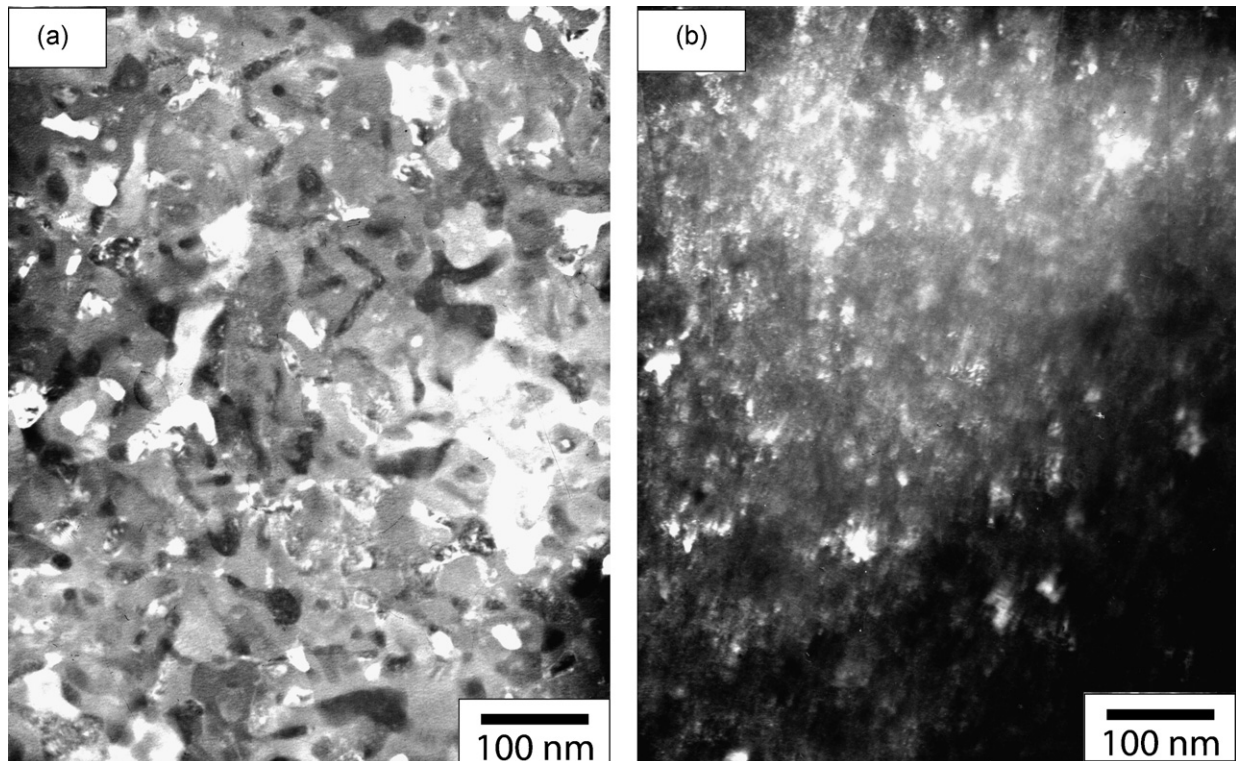


Fig. 3. TEM micrographs of grain morphology of the ribbons melt-spun at the optimum wheel speed of 20 m/s: $\text{Pr}_8\text{Fe}_{86.4}\text{B}_5\text{Cu}_{0.6}$ ribbons (a) and $\text{Pr}_8\text{Fe}_{86.4}\text{B}_5\text{Mn}_{0.6}$ ribbons (b).

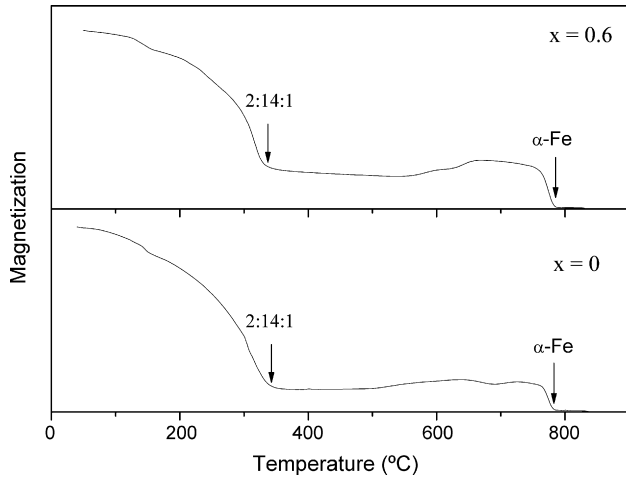


Fig. 4. Temperature dependence of magnetization of $\text{Pr}_8\text{Fe}_{87-x}\text{B}_5\text{Mn}_x$ ribbons with $x=0$ and 0.6 melt-spun at the optimum wheel speed of 20 m/s .

x . For all ribbons, magnetic measurement is parallel to the ribbon planes. For $\text{Pr}_8\text{Fe}_{87-x}\text{B}_5\text{Cu}_x$ ribbons, magnetic properties are also measured perpendicular to the ribbon planes by using a demagnetization factor of 1 , but the measured results along two directions are almost the same, and the B_r value of $\text{Pr}_8\text{Fe}_{87-x}\text{B}_5\text{Cu}_x$ ribbons with c -axis texture are not enhanced by the alignment of $\text{Pr}_2\text{Fe}_{14}\text{B}$ as it was predicted by theoretical calculation [1]. Our recent experiments have shown that the incompletely textured structure in melt-spun $\text{Pr}_2\text{Fe}_{14}\text{B}/\alpha\text{-Fe}$ ribbons does not bring about remanence enhancement [18]. As mentioned above, the texture of $\text{Pr}_2\text{Fe}_{14}\text{B}$ phase in the free

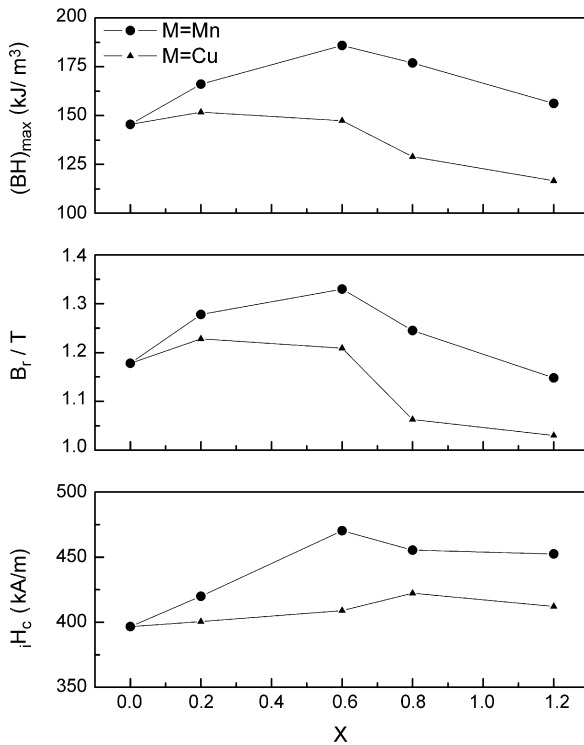


Fig. 5. Room-temperature coercive field iH_c , remanence B_r and maximum energy product $(BH)_{\max}$ of melt-spun $\text{Pr}_8\text{Fe}_{87-x}\text{B}_5\text{M}_x$ ($M=\text{Cu}, \text{Mn}$) ribbons as a function of M concentration x .

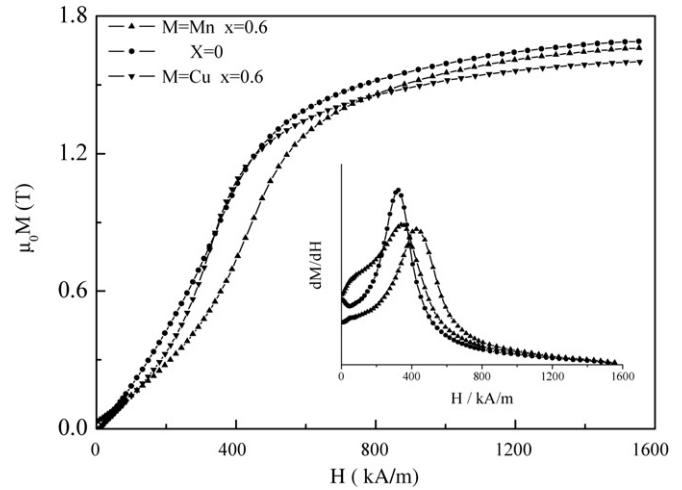


Fig. 6. The initial magnetization curves of $\text{Pr}_8\text{Fe}_{87-x}\text{B}_5\text{M}_x$ ($M=\text{Cu}, \text{Mn}; x=0, 0.6$) ribbons melt-spun at the optimum wheel speed of 20 m/s .

surface does not penetrate through the thickness of melt-spun ribbons because of high cooling rate in the roller surface, so the surface c -axis texture does not result in remanence enhancement.

It can be seen that coercivity of ribbons is improved by the substitution of Cu or Mn , but remanence of ribbons have maximum values when the content of Cu and Mn reaches 0.2 and 0.6 , respectively. Like the addition of other transition metal such as V , Cr , Nb and Zr [8–10], the substitution of Cu improves iH_c but with a significant decrease in B_r . However, Mn substitution of appropriate amount has good effects to both iH_c and B_r of the ribbons. In comparison with Cu substitution, the substitution of Mn improves significantly the B_r and $(BH)_{\max}$ of melt-spun $\text{Pr}_8\text{Fe}_{87-x}\text{B}_5\text{Mn}_x$ ribbons, which mainly resulted from the stronger exchange-coupling effect due to fineness of grain caused by Mn substitution. As shown in Fig. 3, the Cu -doped ribbons show a rather different morphology from that of Mn -doped ribbons. The $2:14:1$ phases in Cu -doped ribbons seem to be oriented, so the grain shape of the $2:14:1$ phase is not well-defined. However, Mn -doped ribbons show a uniform microstructure with ultrafine grains of hard and soft phases, which may lead to the stronger intergranular exchange-coupling effect between the two phases. Due to magnetic dilute effect of nonmagnetic element Cu , the J_s value decreases from 1.68 T for $\text{Pr}_8\text{Fe}_{87}\text{B}_5$ ribbons prepared in our experiments to 1.61 T for $\text{Pr}_8\text{Fe}_{86.4}\text{B}_5\text{Cu}_{0.6}$ ribbons. While the J_s value of $\text{Pr}_8\text{Fe}_{86.4}\text{B}_5\text{Mn}_{0.6}$ decreases to 1.65 T , slightly higher than that of $\text{Pr}_8\text{Fe}_{86.4}\text{B}_5\text{Cu}_{0.6}$.

Studies have shown that replacement of Fe by Mn in $\text{R}_2\text{Fe}_{14-x}\text{Mn}_x\text{B}$ ($\text{R}=\text{Nd}, \text{Pr}$) systems leads initially to an increase in their anisotropy field H_A [19,20]. So the substitution of Mn may lead to an increase of H_A in $\text{Pr}_2(\text{Fe}, \text{Mn})_{14}\text{B}/\alpha\text{-Fe}$ nanocomposites, which may result in the significant enhancement of coercivity in $\text{Pr}_8\text{Fe}_{87-x}\text{B}_5\text{Mn}_x$ ribbons. The initial magnetization curves of $\text{Pr}_8\text{Fe}_{87-x}\text{B}_5\text{M}_x$ ($M=\text{Cu}, \text{Mn}; x=0, 0.6$) ribbons melt-spun at the optimum wheel speed of 20 m/s are shown in Fig. 6. The inset presents $dM/dH-H$ curves of the specimens. In the $dM/dH-H$ curve, the observed sharp peak is associated with the critical value, which is comparable to the

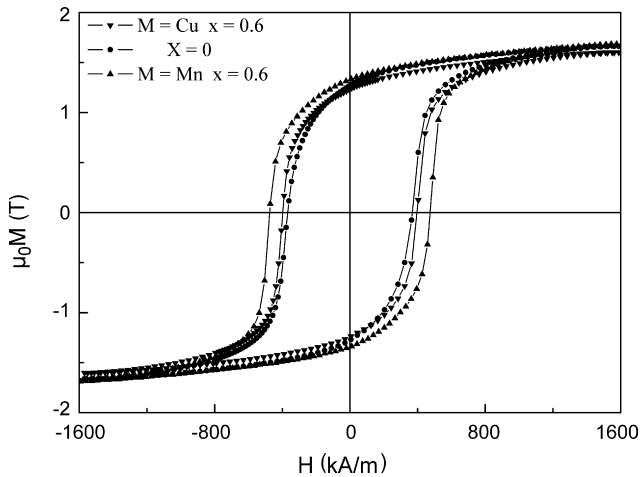


Fig. 7. Room-temperature hysteresis loops of $\text{Pr}_8\text{Fe}_{87-x}\text{B}_5\text{Mn}_x$ ($M=\text{Cu}, \text{Mn}; x=0, 0.6$) ribbons melt-spun at the optimum wheel speed of 20 m/s.

corresponding coercivity. For Mn-doped specimen, the critical value of the specimen is greatly increased. As shown in Fig. 6, the pinning characteristic in the initial magnetization curve for the $\text{Pr}_8\text{Fe}_{86.4}\text{B}_5\text{Mn}_{0.6}$ specimen is more distinct than the others, which implies that the coercivity of the Mn-doped specimens is primarily governed by domain wall pinning [21,22]. It has been shown that a slight substitution of Mn for Fe in $\text{Nd}_2(\text{Fe}_{1-x}\text{Mn}_x)_{14}\text{B}$ with $x \leq 0.3$ increases the strength of the pinning potential barrier during domain wall movement [23]. So the replacement of Fe by Mn may also lead to the improvement of intrinsic magnetic properties of hard magnetic phase $\text{Pr}_2(\text{Fe}, \text{Mn})_{14}\text{B}$ in the $\text{Pr}_8\text{Fe}_{86.4}\text{B}_5\text{Mn}_{0.6}$ ribbons, which results in the distinct pinning characteristics during magnetization.

Fig. 7 shows the typical hysteresis loops of $\text{Pr}_8\text{Fe}_{87-x}\text{B}_5\text{Mn}_x$ ($M=\text{Cu}, \text{Mn}; x=0, 0.6$) ribbons melt-spun at the optimum wheel speed of 20 m/s. The $\text{Pr}_8\text{Fe}_{86.4}\text{B}_5\text{Mn}_{0.6}$ ribbons have a remanence ratio of 0.81 and also have a good squareness in hysteresis loop. A room-temperature remanence $B_r = 1.33$ T, a coercive field $iH_c = 462$ kA/m and a maximum energy product $(\text{BH})_{\text{max}} = 185$ kJ/m³ are obtained in $\text{Pr}_8\text{Fe}_{86.4}\text{B}_5\text{Mn}_{0.6}$ ribbons.

According to the above results, it can be seen that both Cu and Mn of appropriate amount mainly influence the process of rapid solidification of the alloys so that they have different effects on the microstructure of the melt-spun ribbons. The Cu substitution of appropriate quantity probably detains the nucleation and growth of α -Fe crystallites, consequently to promote $\text{Pr}_2\text{Fe}_{14}\text{B}$ phase crystallize competitively and grow up perpendicular to the free surface of the ribbons due to heat flow induced by the contact of the alloys and surface of Cu wheel during melt spinning. But the surface texture does not bring about remanence enhancement. Otherwise, the surface texture makes $\text{Pr}_2\text{Fe}_{14}\text{B}$ grain coarser in $\text{Pr}_8\text{Fe}_{87-x}\text{B}_5\text{Cu}_x$ ribbons. On the contraries, Mn substitution makes the grain sizes of $\text{Pr}_2\text{Fe}_{14}\text{B}$ phase finer, which strengthens the exchange-coupling interaction between hard and soft magnetic phases. The replacement of Fe by Mn in $\text{Pr}_2(\text{Fe}, \text{Mn})_{14}\text{B}$ possibly leads to the increase of intrinsic coercivity of $\text{Pr}_2(\text{Fe}, \text{Mn})_{14}\text{B}$ phase in $\text{Pr}_8\text{Fe}_{87-x}\text{B}_5\text{Mn}_x$ ribbons. These result in significant improvement of magnetic performances of

the $\text{Pr}_8\text{Fe}_{87-x}\text{B}_5\text{Mn}_x$ ribbons. In our previous work, Ga addition has been also found to effectively refine the grain sizes of magnetic phases in nanocomposite $\text{Pr}_2(\text{Fe}, \text{Co})_{14}\text{B}/\alpha$ -(Fe, Co) ribbons and greatly enhance both the remanence and coercivity of the ribbons [6], but the saturation magnetization of the alloys by Ga addition decreases greatly than Mn substitution. Compared with effects of some heavy rare earth elements such as Tb and Dy additive [11,12], which intensify coercivity of the ribbons mostly because of their high magnetocrystalline anisotropy, but weaken remanence seriously, the Mn substitution of appropriate amount do not impair seriously the integrated magnetic performances of nanocomposite alloys.

4. Summary

The structure and magnetic properties of melt-spun $\text{Pr}_8\text{Fe}_{87-x}\text{B}_5\text{Mn}_x$ ($M=\text{Cu}, \text{Mn}; x=0-1.2$) ribbons were studied. An appropriate amount of Cu substitution promotes the c -axis alignment of $\text{Pr}_2\text{Fe}_{14}\text{B}$ phase in the melt-spun ribbons of $\text{Pr}_8\text{Fe}_{87-x}\text{B}_5\text{Cu}_x$, which likely results from delay of nucleation and growth of α -Fe caused by the substitution of Cu. The substitution of Mn leads to the increase of magnetic performances of melt-spun $\text{Pr}_8\text{Fe}_{87-x}\text{B}_5\text{Mn}_x$ ribbons mainly due to finer grain sizes and uniform microstructure. The optimal room-temperature remanence of 1.33 T, coercive field of 462 kA/m and maximum energy product of 185 kJ/m³ are obtained in $\text{Pr}_8\text{Fe}_{86.4}\text{B}_5\text{Mn}_{0.6}$ ribbons melt-spun at the optimum wheel speed of 20 m/s.

Acknowledgements

This work was supported by the National Nature Science Foundation of China and the National Basic Research Program of China.

References

- [1] R. Skomski, J.M.D. Coey, Phys. Rev. B 48 (1993) 15812.
- [2] B.Z. Cui, X.K. Sun, W. Liu, Z.D. Zhang, D.Y. Geng, X.G. Zhao, J.P. Liu, D.J. Sellmyer, J. Appl. Phys. 87 (2000) 5335.
- [3] J. Zhang, S.Y. Zhang, H.W. Zhang, B.G. Shen, J. Appl. Phys. 89 (2001) 5601.
- [4] W.C. Chang, D.Y. Chiou, S.H. Wu, B.M. Ma, C.O. Bounds, Appl. Phys. Lett. 72 (1998) 121.
- [5] I. Betancourta, H.A. Davies, Appl. Phys. Lett. 87 (2005) 162516.
- [6] W.Y. Zhang, J. Zhang, Z.H. Chen, S.Y. Zhang, B.G. Shen, J. Phys.: Condens. Mater. 13 (2000) 3859.
- [7] Z.Q. Jin, H. Okumura, Y. Zhang, H.L. Wang, J.S. Munoz, G.C. Hadjipanayis, J. Magn. Mater. 248 (2002) 216.
- [8] M. Uehara, S. Hirotsawa, H. Kanekiyo, N. Sano, T. Tomida, Nanostruct. Mater. 10 (1998) 151.
- [9] C.J. Yang, E.B. Park, Y.S. Hwang, E.C. Kim, J. Magn. Mater. 212 (2000) 168.
- [10] N.J. Harrison, H.A. Davis, I. Todd, J. Appl. Phys. 99 (2006) 504.
- [11] Z.C. Wang, M.C. Zhang, F.B. Li, S.Z. Zhou, R. Wang, W. Gong, J. Appl. Phys. 81 (1997) 5097.
- [12] Z.Q. Jin, H. Okumura, H.L. Wang, G.C. Hadjipanayis, J. Appl. Phys. 91 (2000) 8165.
- [13] X.Y. Zahng, Y. Guan, L. Yang, J.W. Zhang, Appl. Phys. Lett. 79 (2001) 2426.

- [14] Z.C. Wang, M.C. Zhang, S.Z. Zhou, Y. Qiao, R. Wang, *J. Alloy Compd.* 309 (2000) 212.
- [15] M. Marinescu, H. Chirac, *J. Optoelectron. Adv. Mater.* 4 (2002) 267.
- [16] M. Marinescu, H. Chirac, M. Grigoras, *J. Magn. Magn. Mater.* 290–291 (2000) 1267.
- [17] S. Hirose, Y. Shigemoto, T. Miyoshi, H. Kanekiyo, *Scripta Mater.* 48 (2003) 839.
- [18] B. Yang, B.G. Shen, T.Y. Zhao, J.R. Sun, *Acta Phys. Sin.* 56 (2007) 3527.
- [19] M.Q. Huang, E.B. Boltich, W.E. Wallace, E. Oswald, *J. Less-Common Met.* 124 (1986) 55.
- [20] M. Jurczyk, W.E. Wallace, *IEEE Trans. Magn.* MAG-22 (1986) 755.
- [21] H.W. Zhang, Z.G. Sun, S.Y. Zhang, B.S. Han, B.G. Shen, *Phys. Rev. B* 60 (1999) 64.
- [22] H.W. Zhang, S.Y. Zhang, B.G. Shen, *Phys. Rev. B* 62 (2000) 8642.
- [23] Y.C. Yang, X.D. Zhang, *Acta Phys. Sin.* 39 (1999) 649.